Cell Communication and Signaling

RESEARCH

Open Access

Nuclear basket nucleoporin MoNup50 is essential for fungal development, pathogenicity, and autophagy in *Magnaporthe oryzae*

Ying-Ying Cai[1], Xue-Ming Zhu[1], Muhammad Noman[1], Jing Wang[1], Zhong-Na Hao[1], Yan-Li Wang[1], Lin Li[1], Xiao-Hong Liu[2], Jian-Ping Lu[3], Jiao-Yu Wang[1*] and Fu-Cheng Lin[1,2*]

Abstract

Autophagy is crucial for appressorium development and host invasion by phytopathogenic fungi, including *Magnaporthe oryzae*. During appressorium maturation, many organelles, such as nuclei, in the conidia need to be degraded through autophagy to be recycled in appressorium. However, the interplay between autophagy and nuclear membrane systems remains poorly understood. In this study, we functionally characterized MoNup50, a nuclear pore-associated protein. Despite sharing limited sequence identity with human and yeast Nup proteins, MoNup50 contains conserved domains typical of nuclear pore complex proteins. Observation under fluorescence microscopy revealed that MoNup50 localizes at the nuclear membrane in *M. oryzae*. Deletion of *MoNUP50* resulted in reduced hyphal growth, spore production, appressorium formation, and pathogenicity, while increasing sensitivity to osmotic stress and cell wall disruption. Notably, MoNup50 interacts with the key autophagy protein MoAtg7, which regulates MoAtg8-PE synthesis during autophagy. Moreover, *MoNUP50* deletion led to elevated autophagy levels and increased phosphorylation of the MAPKs Osm1 and Mps1. These findings suggest that MoNup50 is involved in appressorium morphogenesis and pathogenicity by modulating autophagy and MAPK pathways, highlighting the critical role of nuclear pore proteins in *M. oryzae* pathogenicity and their potential cross-talk with autophagic and MAPK signaling.

Keywords Rice blast fungus, Virulence, Atg7, Nuclear pore complex

Introduction

Rice blast, caused by the fungal pathogen *Magnaporthe oryzae*, is one of the most devastating rice diseases, often referred to as the "cancer of rice". It seriously affects global food production and security [1, 2]. *M. oryzae* primarily infects rice through conidia, which are dispersed by wind and rain. Upon landing on the host leaf surface, the conidium germinates to form an infection structure called an appressorium [3]. During appressorium maturation, glycogen and lipid droplets in the conidia translocate to the appressoria. Subsequently, these glycogen and lipid droplets are gradually degraded in appressoria, leading to the accumulation of substantial glycerol and

*Correspondence:
Jiao-Yu Wang
wangjiaoyu78@sina.com
Fu-Cheng Lin
fuchenglin@zju.edu.cn
[1] State Key Laboratory for Quality and Safety of Agro-products, Key Laboratory of Agricultural Microbiome (MARA), Key Laboratory of Agricultural Microbiomes of Zhejiang Province, Key Laboratory of Biotechnology in Plant Protection of MARA, Institute of Plant Protection and Microbiology, Zhejiang Academy of Agricultural Sciences, Hangzhou 310021, China
[2] State Key Laboratory for Quality and Safety of Agro-Products, Key Laboratory of Agricultural Microbiomics of Zhejiang Province, Institute of Biotechnology, Zhejiang University, Hangzhou 310058, China
[3] College of Life Science, Zhejiang University, Hangzhou 310058, China

turgor pressure as high as 8.0 MPa [4]. This turgor pressure drives the formation of penetration pegs, enabling the fungus to breach the host leaf surface and establish infection [5].

Autophagy is a conserved cellular process in which autophagosomes engulf damaged macromolecules and organelles, transporting them to vacuoles or lysosomes for degradation [6, 7]. This process maintains cellular homeostasis by recycling macromolecules to replenish energy and material [8, 9]. During appressorium maturation, conidia undergo autophagy-dependent nuclear degradation, leading to conidial cell death and recycling of conidial contents into appressorium to facilitate turgor pressure generation [10]. Autophagy is regulated by a series of autophagy-related genes (*ATG*s), including *ATG7*, which regulates autophagy by facilitating the formation of autophagosomes through the Atg8-PE synthesis pathway [11].

Nuclear pore complexes (NPCs) are large protein assemblies embedded in the nuclear envelope, mediating the transport of biomolecules between the cytoplasm and nucleus [12, 13]. NPCs consist of seven substructures formed by approximately 30 different nucleoporins (Nups), playing a particularly dynamic structural and functional role. In *Saccharomyces cerevisiae*, Nup2/Nup50 regulates nuclear transport and interacts with chromatin to influence gene expression [12, 14]. Nup2/Nup50 is critical for viability and stress response [15]. In mouse C2 C12 myoblast, Nup2/Nup50 also interacts with active genes in the nucleoplasm, participates in gene regulation, and controls chromatin epigenetic states by preventing the spread of repressive marks [16]. For example, in *Aspergillus nidulans*, Nup2/Nup50 is critical for the cell viability [17]. Similarly, Nup2/Nup50 has been reported to be involved in growth and development, stress response, pathogenicity, and DON toxin synthesis in *Fusarium graminearum* [18].

Recent studies linked the NPC complex to autophagy regulation. In *S. cerevisiae*, TORC1 (Tor kinase complex 1) inhibition triggers autophagic degradation of NPC complex and Nups, mediated by selective autophagic receptors such as Atg8 [19]. In mammals, the nuclear basket Nup, Tpr, regulates autophagy by modulating the export of mRNAs and interacting with autophagy factors [20].

Despite extensive studies in yeast and other organisms, the role of Nup50/Nup2 in *M. oryzae*, especially in autophagy, remains underexplored. In this study, we characterized MoNup50, a nuclear pore-associated protein, essential for hyphal growth, sporulation, appressorium formation, and pathogenicity. MoNup50 also responds to osmotic and cell wall stress by regulating the Osm1 and Mps1 MAPK signaling pathways. Notably, MoNup50 interacts with the key autophagy protein MoAtg7 to regulate autophagy, and deletion of *MoNUP50* resulted in abnormal autophagic activity.

Results

Identification and structural analysis of MoNup50

All analyzed Nup50 homologs, including those from fungi, mammals, and plants, contain the nuclear pore complex protein conserved domain and Nup50 Ran-binding domain, supporting their functional conservation across species (Figure S1 A). Protein structure prediction revealed that fungal (*M. oryzae*, *F. graminearum, S. cerevisiae*, *Schizosaccharomyces pombe*, etc.) and mammalian (*Homo sapiens*, *Xenopus laevis*, *Mus musculus*, etc.) homologs possess two conserved alpha-helices in their core regions. In contrast, plant homologs (*O. sativa*, *H. vulgare*, *A. thaliana*) exhibit only one alpha-helix in the same region (Fig. 1). Phylogenetic analysis of Nup50 from various organisms showed that MoNup50 of *M. oryzae* is more closely related to Nup50 in most other fungi than to plants (*O. sativa*, *H. vulgare*, *A. thaliana*) and mammals (*H. sapiens*, *X. laevis*, *Mus musculus*, *Rattus norvegicus*) (Figure S1B).

Using a homologous recombination-based gene knockout strategy, we knocked out *MoNUP50* in the *M. oryzae* strain Guy11. Successful deletion of *MoNUP50* was confirmed by polymerase chain reaction (PCR) and quantitative real-time polymerase chain reaction (qRT-PCR) to verify a single-copy insertion of *HPH* (Figure S2). The resulting knockout mutant was designated Δ*Monup50*. To ensure that observed phenotypic alterations in Δ*Monup50* were specifically due to the absence of *MoNUP50*, a complementation strain (Δ*Monup50::MoNUP50*) was generated by reintroducing the full-length *MoNUP50* genomic sequence into the Δ*Monup50* mutant. We also reintroduced the *S. cerevisiae NUP2* ortholog into the Δ*Monup50* mutant (Δ*Monup50::ScNUP2*) and found that *S. cerevisiae NUP2* could partially restore the hyphal growth and pathogenicity defects in the Δ*Monup50* mutant (Figure S3).

MoNup50 localizes at the nuclear envelope in *M. oryzae*

To determine the subcellular localization of MoNup50 in *M. oryzae*, we constructed a GFP-MoNup50 fusion vector and transformed it into Δ*Monup50*. The observation under fluorescence microscopy showed that GFP-MoNup50 localized around the nucleus. Co-localization of GFP-MoNup50 at different developmental stages (hyphae, conidia, and appressoria) with the nuclear marker protein MoH_2B-mCherry showed that GFP-MoNup50 formed a punctate structure around the nucleus in hyphae and a ring-like structure in conidia

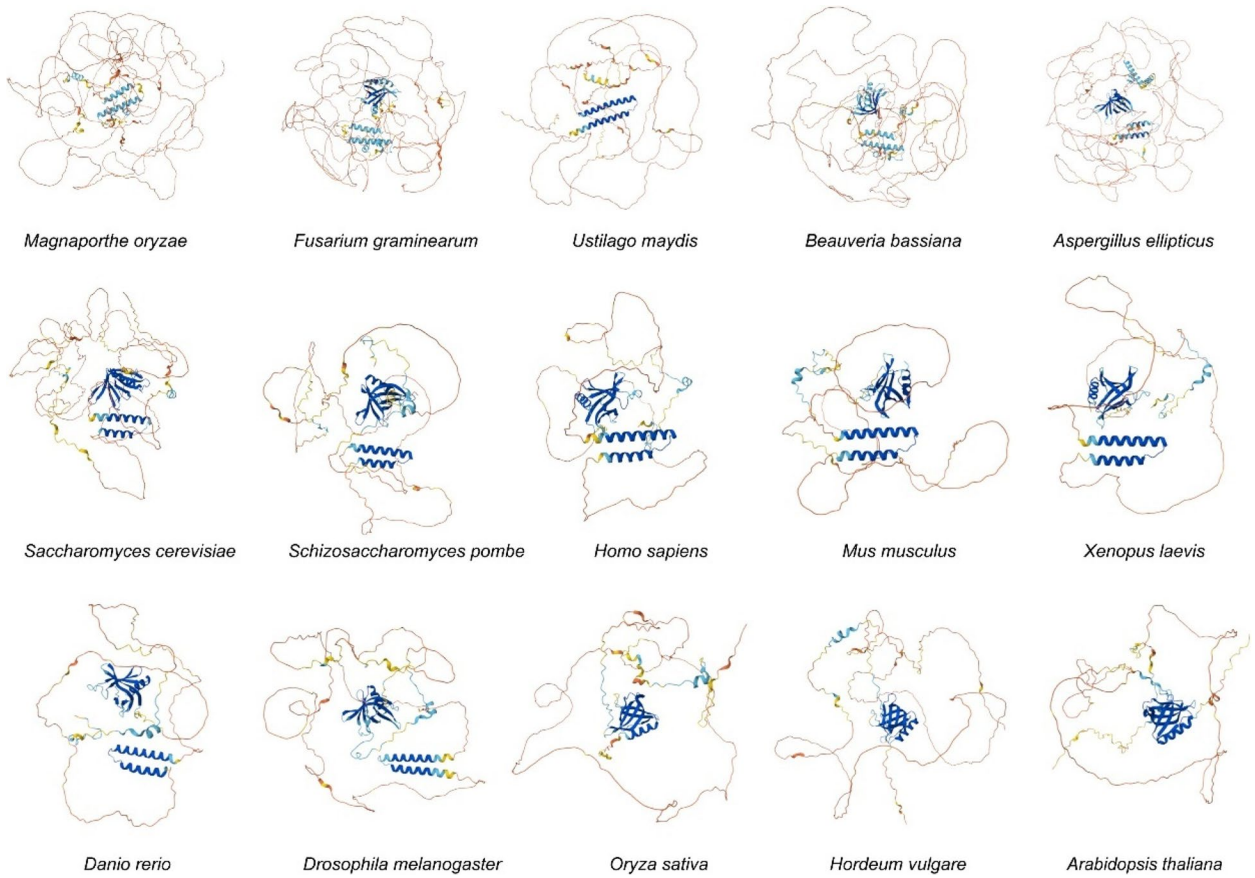

Fig. 1 Prediction of the protein structures of Nup50 across different species using the AlphaFold Protein Structure Database website

and mature appressoria, suggesting MoNup50 localizes at the nuclear envelope (Fig. 2A and B).

MoNup50 regulates hyphal growth, spore production, and spore morphology

To assess the biological function of MoNup50, we examined the hyphal growth, conidiation, and spore morphology. The Δ*Monup50* mutant showed a 41% reduction in colony growth diameter compared to the wild-type (Guy11) and complemented strains (Fig. 3A and D). Sporulation assays revealed that the Δ*Monup50* mutant failed to produce conidia after 24 h, with sporulation reduced by 98% compared to the Guy11 and complemented strains (Fig. 3B and E). Additionally, the conidia from the Δ*Monup50* mutant displayed abnormal morphology, with over 85% showing either no septa or a single septum, whereas more than 90% of Guy11 conidia exhibited two septa (Fig. 3C and F). These results indicate that MoNup50 is essential for vegetative growth, spore morphology, and sporulation.

MoNup50 regulates appressorium formation and appressorium turgor pressure

At 4, 8, and 12 h post-inoculation (hpi), the spores of the Δ*Monup50* mutant exhibited significantly lower appressorium formation rates compared to the Guy11 and complemented strains (Fig. 4A and C). 9.70% of the conidia in the Δ*Monup50* mutant formed appressoria at 4 hpi, compared to over 50% in the Guy11 and complemented strains. At 24 hpi, however, appressorium formation rates were similar between the Δ*Monup50* mutant and the Guy11. When submerged in a highly concentrated glycerol solution, the collapse rate of appressoria in the Δ*Monup50* mutant was significantly higher than in the Guy11 and complemented strains, indicating the mutant's appressoria have lower turgor pressure (Fig. 4B and D). These findings suggest that MoNup50 is crucial for appressorium formation and turgor pressure generation.

MoNup50 is involved in infection and pathogenicity

To examine the role of MoNup50 in pathogenicity, we first inoculated the Δ*Monup50*, Guy11, and complemented strains onto detached barley leaves. At

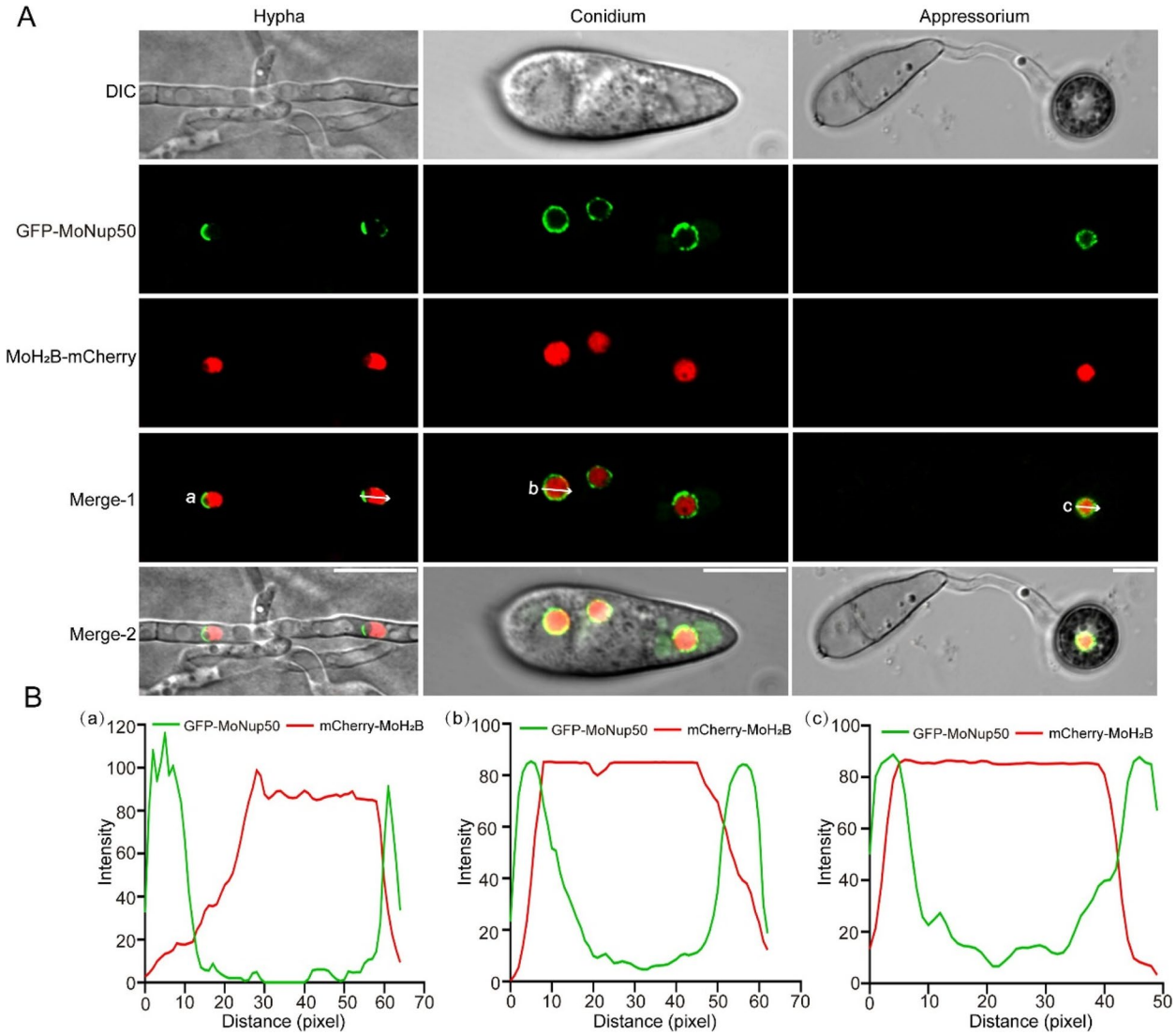

Fig. 2 MoNup50 localizes to the nuclear envelope in *M. oryzae*. **A** Localization of MoNup50 in the hyphae, conidia, and appressoria of *M. oryzae*. Scale bar, 10 μm. **B** The fluorescence intensity of GFP-MoNup50 and mCherry-MoH$_2$B was measured by ImageJ software

4 dpi, the Δ*Monup50* mutant showed few tiny infection lesions, while the Guy11 and complemented strains caused typical coalescent lesions (Fig. 5A). Similarly, spore suspensions were inoculated onto barley leaves, producing only small and restricted lesions by the Δ*Monup50* mutant, while the Guy11 and complemented strains caused large and coalescent lesions (Fig. 5B). In rice seedling infection assays, the Δ*Monup50* mutant caused significantly fewer lesions (lesion area 11.11 ± 0.73%) compared to the Guy11 (78.98 ± 3.26%) and complemented strains (77.32 ± 2.22%) (Fig. 5C and E).

Further analysis of barley leaf infection experiments at 36 and 48 hpi revealed that Δ*Monup50* has defects in plant penetration and invasive growth. The infection hyphae (IH) were classified into three types, Type I (no IH formation, indicating arrested initial infection), and Type II (IH confined to a single host cell), Type III (IH penetrating and spreading to adjacent cells). At 48 hpi, the Δ*Monup50* mutant exhibited severe defects in invasive growth: 84% of infection sites displayed Type I or II hyphae, with only 16% progressing to Type III. In contrast, Guy11 and the complemented strain formed Type III hyphae in ~ 90% of infection sites, demonstrating efficient cell-to-cell spread (Fig. 5D and F). These results indicate that MoNup50 is crucial for full infection and pathogenicity.

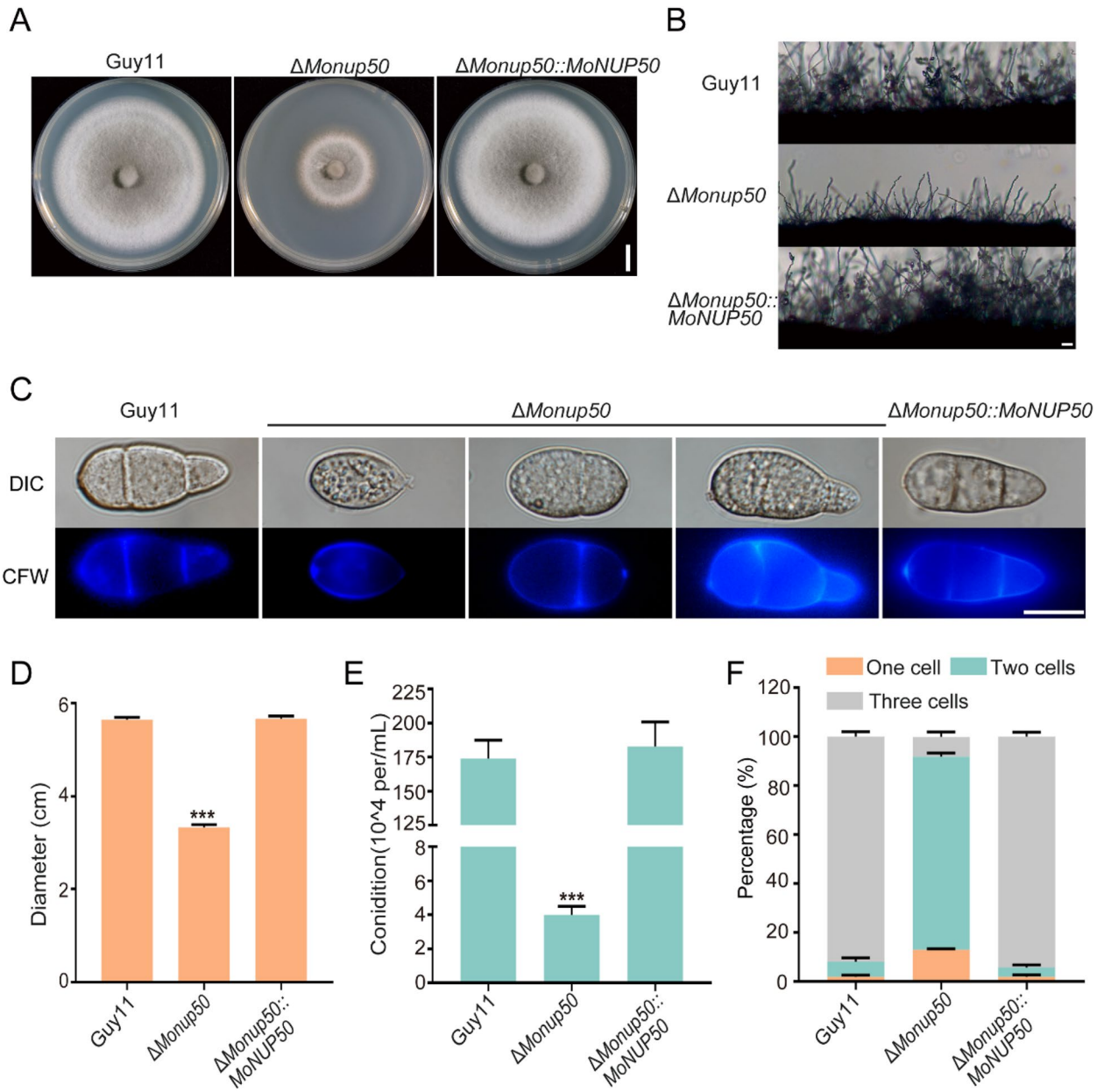

Fig. 3 MoNup50 regulates hyphal growth, spore production, and spore morphology. **A** Hyphal growth of Guy11, Δ*Monup50*, and Δ*Monup50::MoNUP50*. Scale bar, 1 cm. **B** Conidia and conidiophores of Guy11, Δ*Monup50*, and Δ*Monup50::MoNUP50*. Scale bar, 50 μm. **C** Conidia morphology of Guy11, Δ*Monup50*, and Δ*Monup50::MoNUP50*. Scale bar, 10 μm. **D** Count and analyze the colony growth diameter of Guy11, Δ*Monup50*, and Δ*Monup50::MoNUP50*. **E** Statistical analysis of conidiation in Guy11, Δ*Monup50*, and Δ*Monup50::MoNUP50*. **F** Statistical analysis of the conidial septum number of Guy11, Δ*Monup50*, and Δ*Monup50::MoNUP50*. One-way ANOVA was used to determine significance. *** $p < 0.001$

MoNup50 affects stress tolerance and signal transduction pathways

To investigate the role of MoNup50 in environmental stresses, we conducted sensitivity assays in response to osmotic stressors (Sorbitol, NaCl, and KCl) and cell wall stressors (CFW, SDS, and CR). We found that the Δ*Monup50* mutant exhibited increased sensitivity to ionic hyperosmotic stress (NaCl and KCl) and cell wall stress (CFW, SDS, and CR), but no significant change in response to non-ionic hyperosmotic stress (Sorbitol) (Figs. 6A, B, and 7A, C).

The Osm1 MAPK and Mps1 MAPK signaling pathways are central pathways to hyperosmotic and cell wall stress responses in *M. oryzae* [21]. We examined the

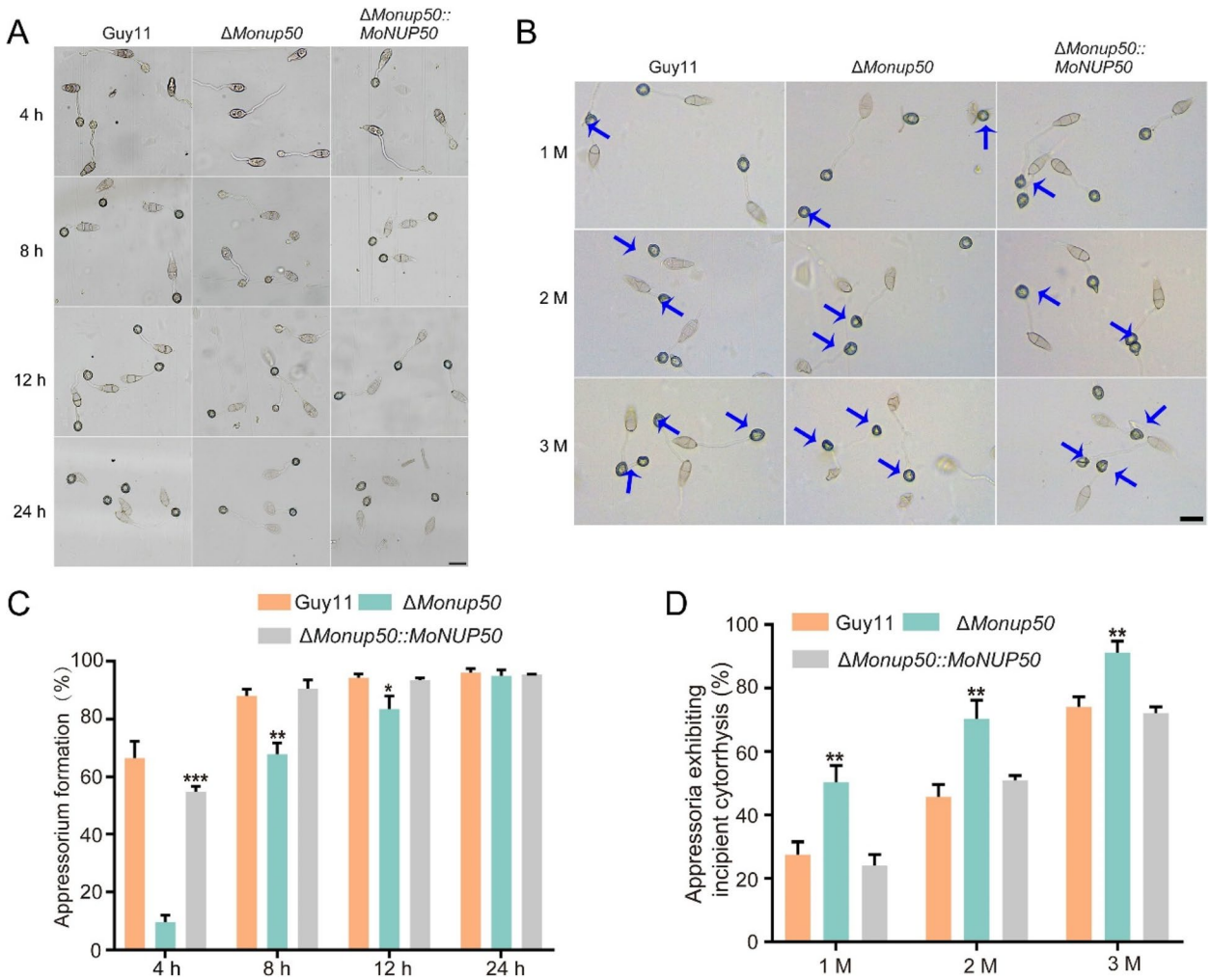

Fig. 4 MoNup50 regulates appressorium formation and appressorium turgor pressure. **A** and **B** appressorium formation and appressorium turgor in Guy11, Δ*Monup50*, and Δ*Monup50::MoNUP50*. The collapsed appressorium is indicated by a blue arrow. Collapse was defined as a loss of turgor pressure and structural integrity. Scale bar, 10 μm. **C** and **D** The appressorium formation rates and appressorium collapse rates of Guy11, Δ*Monup50*, and Δ*Monup50::MoNUP50* were analyzed, respectively. The data were analyzed by unpaired two-tailed Student's t-test (*$p < 0.05$, **$p < 0.01$, *** $p < 0.001$)

phosphorylation levels of Osm1 and Mps1 in the Guy11 and the Δ*Monup50* mutant. Phosphorylation levels of Osm1 and Mps1 were higher in the Δ*Monup50* mutant than in the Guy11 under normal and NaCl- or CR-induced conditions, indicating that MoNup50 modulates these signaling pathways during the stress response (Figs. 6C, D, and 7B, D). These findings suggest that MoNup50 responds to hyperosmotic stress and cell wall stress by regulating the Osm1 and Mps1 MAPK signaling pathways.

MoNup50 affects the transport and degradation of glycogen and lipid droplets

In *M. oryzae*, glycogen and lipid droplets in conidia are degraded and transported to the appressorium via the

(See figure on next page.)

Fig. 5 MoNup50 is involved in infection and pathogenicity. **A** Disease spots of isolated barley leaves inoculated with mycelial plugs of Guy11, Δ*Monup50*, and Δ*Monup50::MoNUP50*. **B** Disease symptoms on isolated barley leaves inoculated conidial suspensions of Guy11, Δ*Monup50*, and Δ*Monup50::MoNUP50*. **C** Rice seedlings inoculated spore suspensions of Guy11, Δ*Monup50*, and Δ*Monup50::MoNUP50*. **D** Penetration assays in isolated barley leaves were separately monitored at different time points. Scale bar, 20 μm. **E** The area occupied by disease spots per 5 cm of rice leaves was counted. **F** Analysis of the number of different invasive hyphae types of Guy11, Δ*Monup50*, and Δ*Monup50::MoNUP50*. One-way ANOVA was used to determine significance. *** $p < 0.001$

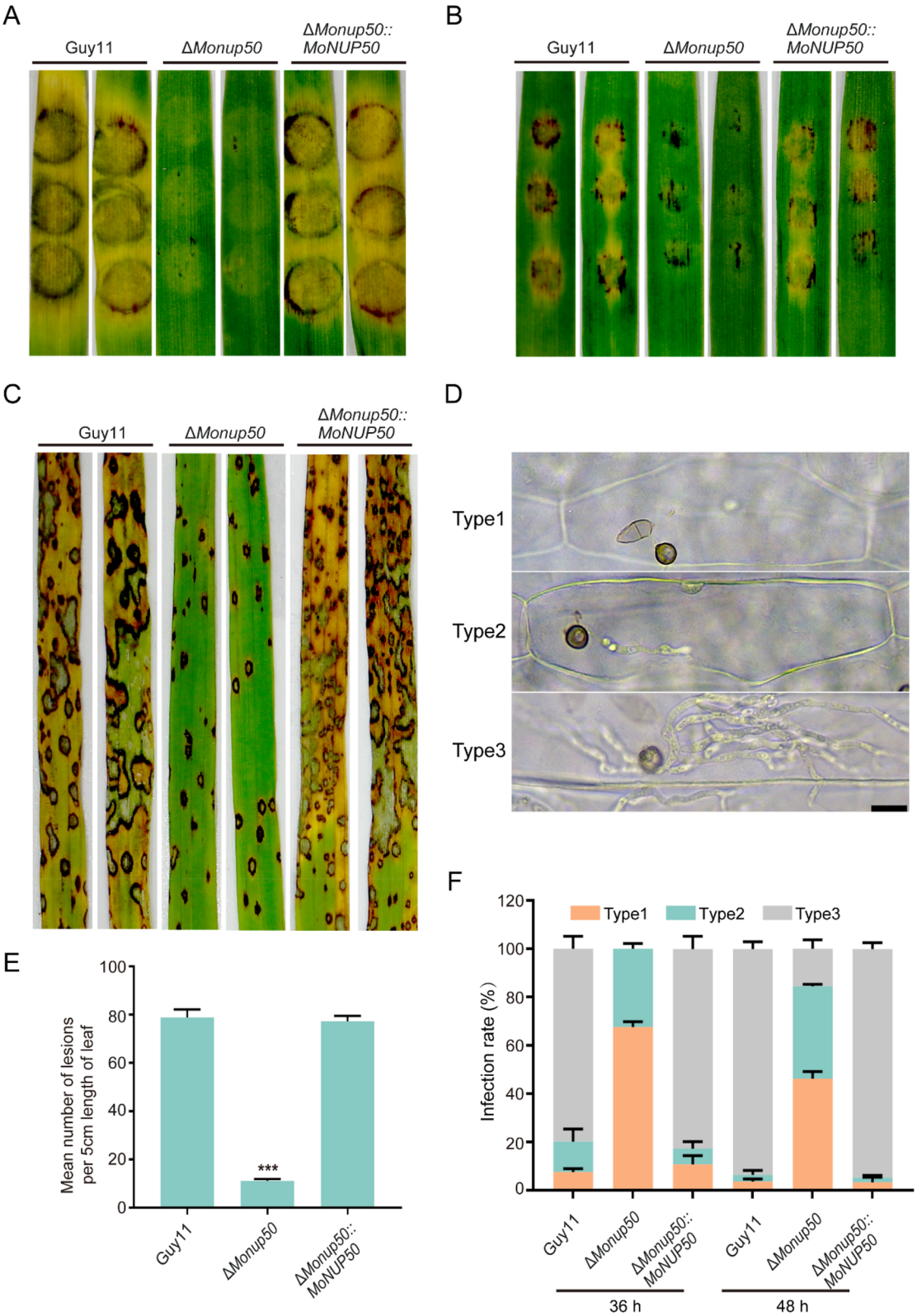

Fig. 5 (See legend on previous page.)

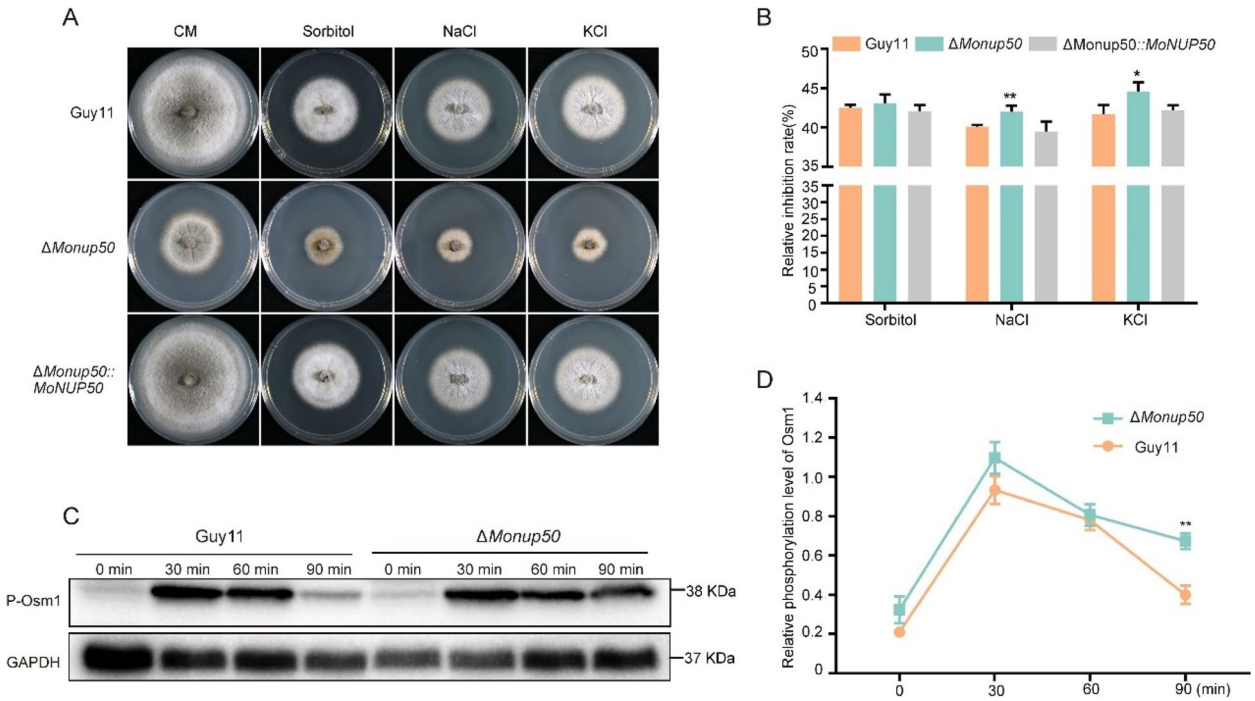

Fig. 6 MoNup50 regulates the phosphorylation of Osm1 in response to hyperosmotic stresses. **A** Colonies of Guy11, Δ*Monup50*, and Δ*Monup50::MoNUP50* on CM supplemented with 1 M Sorbitol, 0.6 M KCl and 0.6 M NaCl. **B** Statistical analysis of growth inhibition rates of Guy11, Δ*Monup50*, and Δ*Monup50::MoNUP50* in plates with different hyperosmotic stress factors. **C** The phosphorylation level of Osm1 in Guy11 and Δ*Monup50* mutants. **D** Statistical analysis of the phosphorylated level of Osm1 in Guy11 and Δ*Monup50*. The data were analyzed by unpaired two-tailed Student's t-test (*$p < 0.05$, **$p < 0.01$)

germ tube, leading to the accumulation of glycerol, which generates the necessary turgor pressure for infection [22]. To assess the cause of reduced turgor pressure in the Δ*Monup50* mutant, we examined the transport and degradation of glycogen and lipid droplets during appressorium development in three strains. At the conidial stage, no significant difference in glycogen synthesis was observed between the Δ*Monup50* mutant and the Guy11. At 8 hpi, 54.12 ± 5.44% conidia of the Δ*Monup50* mutant contained glycogen, whereas only 15.51 ± 3.38% conidia of the Guy11 contained glycogen. At 16 hpi, 93.67% ± 0.65% of the glycogen in the Guy11 appressoria had been degraded, in contrast, less than 30% of the glycogen was degraded in the Δ*Monup50* mutant. These data indicate that MoNup50 regulates glycogen transfer and degradation in the conidia and appressoria of *M. oryzae* (Fig. 8A, B, and C). Intriguingly, there was no significant difference in the transport of lipid droplets in the conidia between the Δ*Monup50* mutant and Guy11. However, lipid droplet degradation in the Δ*Monup50* mutant appressoria was delayed (Fig. 8D, E, and F). These findings suggest that MoNup50 is crucial for the transport of glycogen and the degradation of glycogen and lipid droplets in appressorium.

MoNup50 negatively regulates autophagy

Tor is a key regulator of the autophagy process [23]. Rapamycin is a specific inhibitor of Tor kinase [24]. To investigate the role of MoNup50 in autophagy, we inoculated mycelial plugs of Guy11 and the Δ*Monup50* mutant onto plates containing 100 ng/mL rapamycin and assessed their growth. The Δ*Monup50* mutant showed stronger sensitivity than Guy11 and Δ*Monup50*::*MoNUP50* (Fig. 9A and B). These results suggest that MoNup50 plays a role in regulating autophagy.

To further investigate whether MoNup50 directly influences autophagy, we introduced an autophagy marker GFP-MoAtg8 into the Guy11(Guy11::GFP-MoAtg8, GA8) and the Δ*Monup50* mutant (Δ*Monup50*::GFP-MoAtg8, Δ*Monup50*-A8). We examined the subcellular localization of GFP-MoAtg8 and free GFP (which results from the degradation of GFP-MoAtg8 within vacuoles) using a fluorescence microscope (Fig. 9C). Under nutrient-sufficient conditions, the GFP-MoAtg8 was mainly localized in the cytoplasm in the GA8 hyphae, appearing as bright puncta near the vacuoles. In contrast, in the Δ*Monup50*-A8 hyphae, most of the GFP-MoAtg8 entered the vacuoles, with only a few puncta remaining near the vacuoles in the cytoplasm. At 1 h post-starvation, the GA8 hyphae exhibited GFP-MoAtg8 puncta

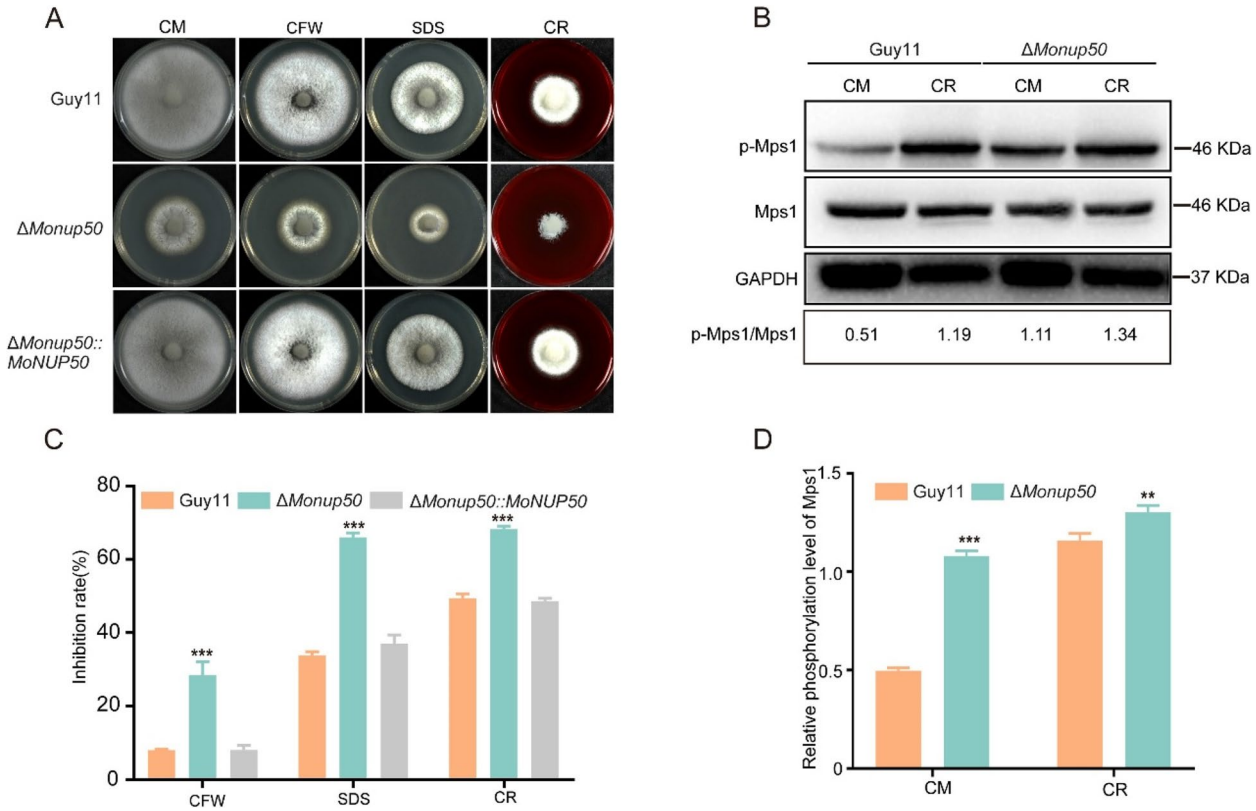

Fig. 7 MoNup50 regulates the Mps1 phosphorylation level in response to cell wall stress. **A** Colonies of Guy11, Δ*Monup50* and Δ*Monup50::MoNUP50* on CM with 50 μg/mL Calcofluor White (CFW), 0.005% SDS and 600 μg/mL Congo Red (CR). **B** The phosphorylation level of Mps1 in Guy11 and Δ*Monup50* on 600 μg/mL CR. **C** Statistical analysis of growth inhibition rates of Guy11, Δ*Monup50* and Δ*Monup50::MoNUP50* in plates with different cell wall stress factors. **D** Statistical analysis of the relative phosphorylation level of Mps1 in Guy11 and Δ*Monup50*. The data were analyzed by unpaired two-tailed Student's t-test (** $p < 0.01$, *** $p < 0.001$)

near the vacuoles, with additional degradation into free GFP within the vacuoles. However, in the Δ*Monup50*-A8 hyphae, all GFP-MoAtg8 degraded into free GFP diffusely distributed within the vacuoles, with no punctate fluorescence observed in the cytoplasm.

Autophagy is also crucial for conidia germination, during which intracellular proteins, macromolecules, and damaged organelles are degraded for cellular recycling. We assessed the autophagy level in the Δ*Monup50*-A8 at spore germination stages by monitoring GFP-MoAtg8 localization (Fig. 9D). Under nutrient-sufficient conditions, GFP-MoAtg8 in the GA8 was mainly distributed as punctate fluorescence in the cytoplasm, with minimal diffuse fluorescence of free GFP in the vacuoles, indicating a low autophagy level. In contrast, in the Δ*Monup50*-A8, only a few punctate GFP-MoAtg8 signals were observed in the cytoplasm, with the majority degrading into free GFP in the vacuoles, indicating a higher autophagy level. At 1–2 h post-starvation, the Guy11 exhibited a decrease in punctate GFP-MoAtg8 signals and an increase in free GFP signals within vacuoles, indicating an increase in autophagy with prolonged starvation. In contrast, the Δ*Monup50*-A8 displayed almost no punctate GFP-MoAtg8 in the cytoplasm, with the majority of GFP-MoAtg8 degrading into free GFP and accumulating in vacuoles. We further investigated

(See figure on next page.)

Fig. 8 MoNup50 impairs glycogen and lipid droplet metabolism in appressoria. **A** Glycogen distribution in conidia and appressoria of Guy11, Δ*Monup50*, and Δ*Monup50::MoNUP50*. Scale bar, 10 μm. **B** and (**C**) The percentage of conidia and appressoria containing glycogen in Guy11, Δ*Monup50*, and Δ*Monup50::MoNUP50*, respectively. **D** Lipid droplets distribution in conidia and appressoria of Guy11, Δ*Monup50*, and Δ*Monup50::MoNUP50*. Scale bar, 10 μm. **E** and **F** The percentage of conidia and appressoria containing lipid droplets in Guy11, Δ*Monup50*, and Δ*Monup50::MoNUP50*, respectively. The data were analyzed by unpaired two-tailed Student's t-test (** $p < 0.01$, *** $p < 0.001$)

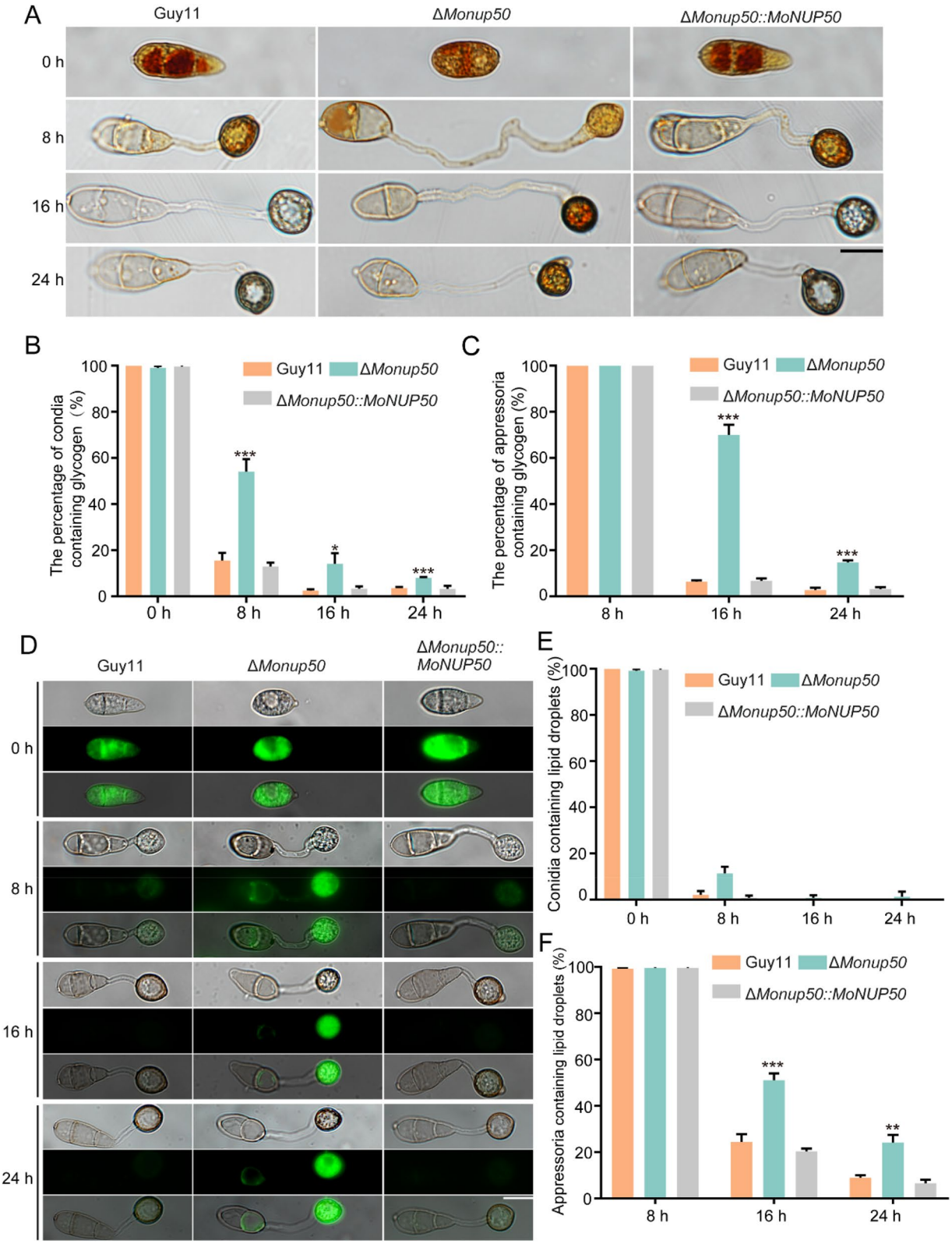

Fig. 8 (See legend on previous page.)

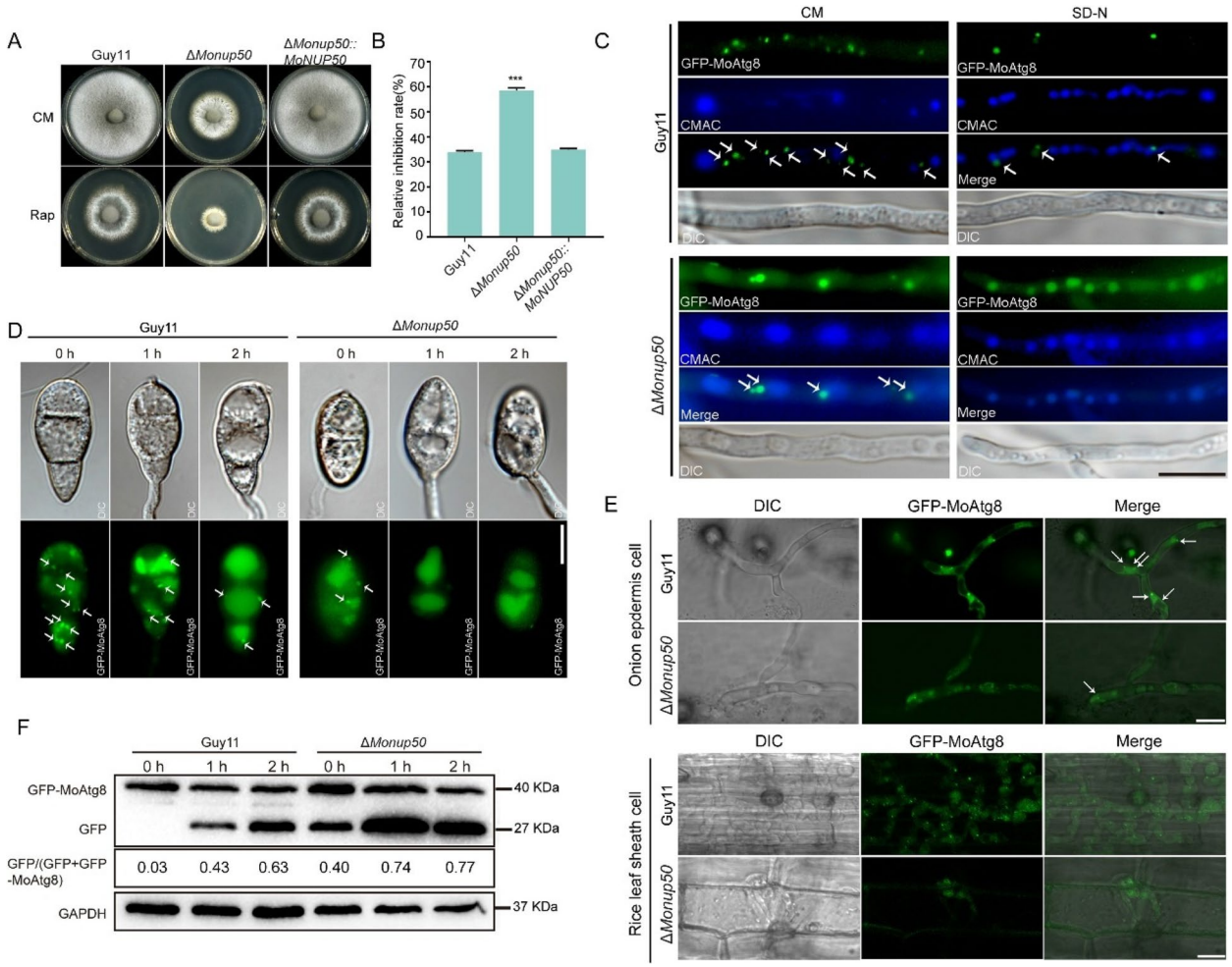

Fig. 9 MoNup50 negatively regulates autophagy. **A** Growth of the Guy11, Δ*Monup50*, and Δ*Monup50::MoNUP50* on CM with 100 ng/mL rapamycin. **B** The relative growth inhibition rates of Guy11, Δ*Monup50*, and Δ*Monup50::MoNUP50* on CM supplemented with 100 ng/mL rapamycin were analyzed. The data were analyzed by unpaired two-tailed Student's t-test (*** $p < 0.001$). **C** The localization of GFP-MoAtg8 in the hyphae of Guy11 and Δ*Monup50*. Scale bar, 10 μm. **D** The localization of GFP-MoAtg8 in the conidia of Guy11 and Δ*Monup50*. Scale bar, 10 μm. **E** The localization of GFP-MoAtg8 in onion epidermal cells and rice sheath cells, respectively. Scale bar, 5 μm. **F** The breakdown of GFP-MoAtg8 of Guy11 and Δ*Monup50*

the subcellular localization of GFP-MoAtg8 in invasive hyphae. In onion epidermal cells and rice sheath cells, the GA8 strain exhibited a higher frequency of punctate GFP-MoAtg8 signals compared to the Δ*Monup50*-A8 mutant (Fig. 9E). In Δ*Monup50*-A8, GFP-MoAtg8 predominantly displayed diffuse localization patterns within these host cellular environments (Fig. 9E). These observations suggest that the autophagy level is higher in the Δ*Monup50* mutant than in the Guy11.

To quantitatively analyze autophagic flux, we performed western blotting to detect GFP-MoAtg8 and free GFP protein levels (Fig. 9F). Under nutrient-rich conditions, a strong band for GFP-MoAtg8 was observed in the GA8, and free GFP was barely detectable. In contrast, GFP-MoAtg8 and free GFP bands were detected at comparable intensities in the Δ*Monup50*-A8 mutant. Specifically, 3% of GFP-MoAtg8 in the GA8 degraded to free GFP, while 40% of GFP-MoAtg8 degraded to free GFP in the Δ*Monup50*-A8 mutant. At 1 h post-starvation, the band for free GFP in the GA8 remained weaker than the GFP-MoAtg8 band, but at 2 h post-starvation, the free GFP band became comparable to the GFP-MoAtg8 band. In contrast, in the Δ*Monup50*-A8 mutant, the free GFP band was stronger than the GFP-MoAtg8 at 1 and 2 h post-starvation. Precisely, 43% and 63% of GFP-MoAtg8 degraded into free GFP in the GA8 at 1 and 2 h post-starvation, respectively. While 74% and

77% of GFP-MoAtg8 degraded into free GFP in the Δ*Monup50*-A8 mutant, respectively. These results indicate that autophagy levels were significantly higher in the Δ*Monup50*-A8 mutant than in the GA8 under nutrient-rich and starvation conditions.

MoNup50 interacts with the key autophagy protein MoAtg7 *in vitro* and *in vivo*

To further validate the relationship between MoNup50 and autophagy, we screened the interaction between MoNup50 and the key autophagy protein, MoAtg7. In yeast two-hybrid assays, we found that co-transforming yeast cells with the MoAtg7-AD plasmid and MoNup50-BD plasmid allowed yeast growth on SD-Leu-Trp-His-Ade plates. However, when the MoAtg7-AD plasmid was co-transformed with the pGBKT7 plasmid or the MoAtg7-AD plasmid was co-transformed with the pGADT7 plasmid into the yeast cells, no growth was observed on SD-Leu-Trp-His-Ade plates, indicating that MoNup50 interacts specifically with MoAtg7 without any self-activation (Fig. 10A). In vitro GST-pull down assays further confirmed the interaction between MoNup50 and MoAtg7. GST-MoAtg7 could pull down His-MoNup50 from the lysate using GST beads, whereas the negative control (empty GST protein) did not pull down any protein (Fig. 10B). These results indicate that MoNup50 and MoAtg7 interact directly in vitro. Additionally, we used the bimolecular fluorescence complementation (BiFC) method to confirm the interaction between MoNup50 and MoAtg7 in vivo. The C-terminal fragment of *MoNUP50* was fused to the pKD5-YFPC vector, and the N-terminal fragment of *MoATG7* was fused to the pKD5-YFPN vector. Both constructs were co-transformed into Guy11. As negative controls, we co-transformed YFPN/MoNup50-YFPC and YFPC/YFPN-MoAtg7 into Guy11. YFP signals were detected in the transformants expressing MoNup50-YFPC/YFPN-MoAtg7, but no fluorescence was observed in the negative controls, confirming that MoNup50 interacts with MoAtg7 in vivo (Fig. 10C). These results demonstrate that in *M. oryzae*, MoNup50 interacts with MoAtg7 in vitro and in vivo.

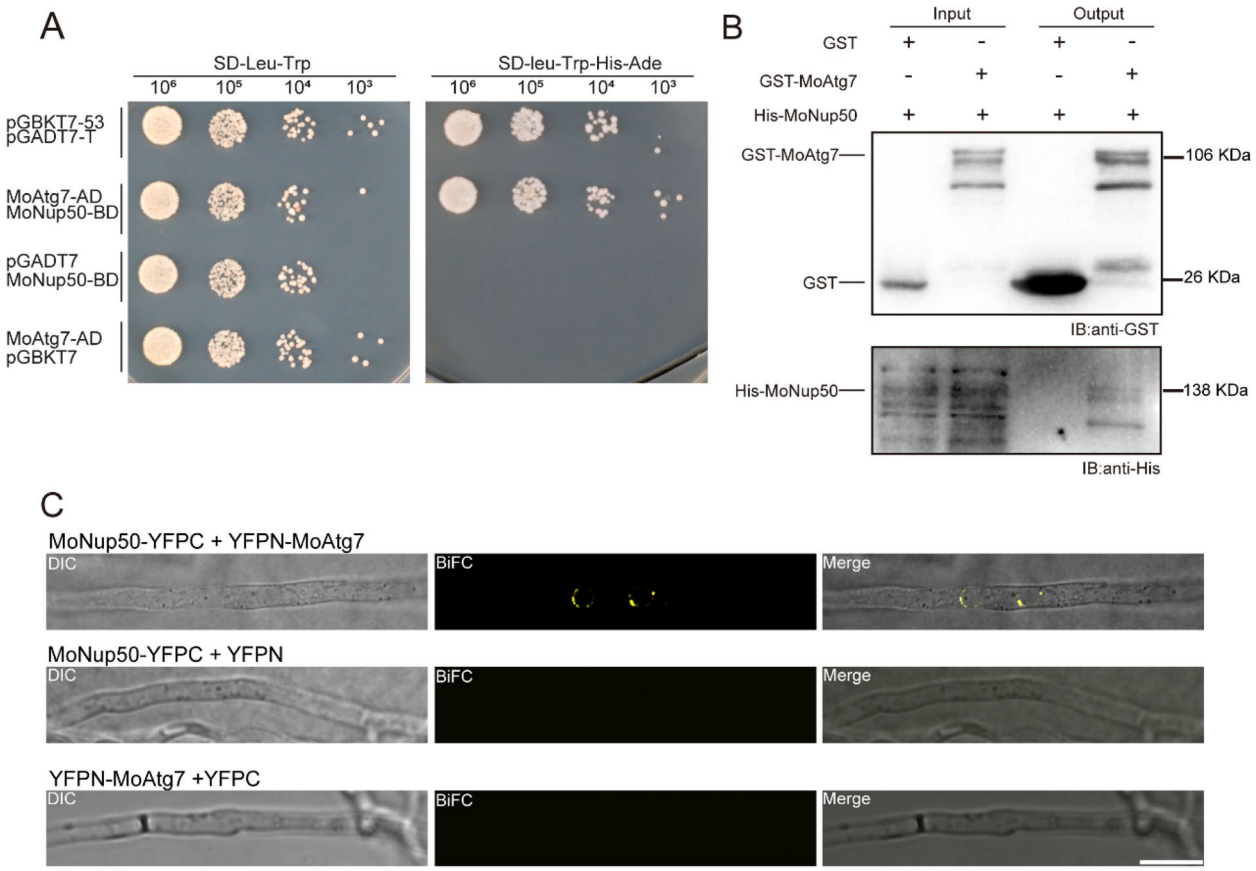

Fig. 10 MoNup50 interacts with the key autophagy protein MoAtg7 in vitro and in vivo. **A** Yeast two-hybrid analysis to examine the interaction between MoNup50 and MoAtg7 in vivo. **B** GST-pull down assay for detecting the interaction between MoNup50 and MoAtg7 in vitro. **C** BiFC assay to detect the interaction between MoNup50 and MoAtg7 in vivo. Scale bar, 10 μm

MoNup50 inhibits the MoAtg8-PE synthesis

To investigate how MoNup50 affects MoAtg7 and its role in the autophagy process, we assessed the relative expression level of MoAtg7 in the Guy11 and the Δ*Monup50* mutant. We found that the expression level of MoAtg7 in the Δ*Monup50* mutant was ~two fold higher than that in the Guy11 (Fig. 11A), suggesting that Monup50 is involved in the regulation of *MoATG7* expression. In the autophagy induction process of *S. cerevisiae*, Atg8 undergoes lipidation, a process catalyzed by a series of enzymes, including Atg4, Atg7, Atg3, and the Atg5-Atg12-Atg16 complex. This results in the formation of Atg8-PE, which is anchored to the autophagosome membrane [25, 26]. Given the close correlation between MoAtg8-PE and the number of autophagosomes [27], we measured the turnover of endogenous MoAtg8 and MoAtg8-PE in the Guy11 and the Δ*Monup50* mutant by western blotting to assess autophagy levels. Results showed that MoAtg8 lipidation levels increased over time in the Guy11 and the Δ*Monup50* mutant under starvation conditions (Fig. 11B). Notably, under nutrient-rich and starvation conditions, the MoAtg8-PE bands were more prominent in the Δ*Monup50* mutant compared to the Guy11. At 2 h post-starvation, the MoAtg8-PE/GAPDH ratio in the Δ*Monup50* mutant reached 1.55, whereas in the Guy11, the ratio was only 0.56 (Fig. 11B). These results suggest that MoNup50 negatively regulates the conversion process of MoAtg8 to MoAtg8-PE.

Discussion

Eukaryotic cells rely on the bidirectional transport of essential substances between the nucleus and cytoplasm. Molecules critical for protein synthesis, such as tRNAs, mRNAs, and pre-ribosomal subunits, are exported from the nucleus to the cytoplasm. In contrast, nuclear proteins, including histones and transcription factors, are imported into the nucleus. This nucleoplasmic transport is mediated by the NPC [28]. Recent studies have highlighted the relationship between the NPC complex and autophagy. In autophagy-impaired cells, the NPC mediates the essential proteins in the cytoplasm to be translocated to the nucleus and degraded [29].

Despite the role of NPC in material transport being well-characterized, its biological functions and relationship with autophagy in plant pathogenic fungi remain poorly understood. In this study, we identified a novel nuclear basket nucleoporin, MoNup50, in *M. oryzae* and investigated its biological functions. Our data revealed that MoNup50 acts as a negative regulator of autophagy. Phenotypic analysis of the Δ*Monup50* mutant further demonstrated that MoNup50 plays an essential role in the conidia and appressoria development, as well as pathogenicity in *M. oryzae* (Fig. 12).

Phenotypic analysis of the Δ*Monup50* mutant revealed that MoNup50 is involved in multiple aspects of fungal development and pathogenicity, including vegetative hyphal growth, spore production, septum formation in conidia, appressorium formation, turgor pressure generation, and the transport and degradation of glycogen and lipid droplets within appressorium. In *M. oryzae*, glycogen and lipid droplets are transported to appressoria, where they are metabolized to produce glycerol. This glycerol accumulates in appressorium, generating turgor pressure that facilitates the formation and penetration of infection pegs into the host plant cuticle, leading to severe infection lesions [30, 31]. In this study, the deletion

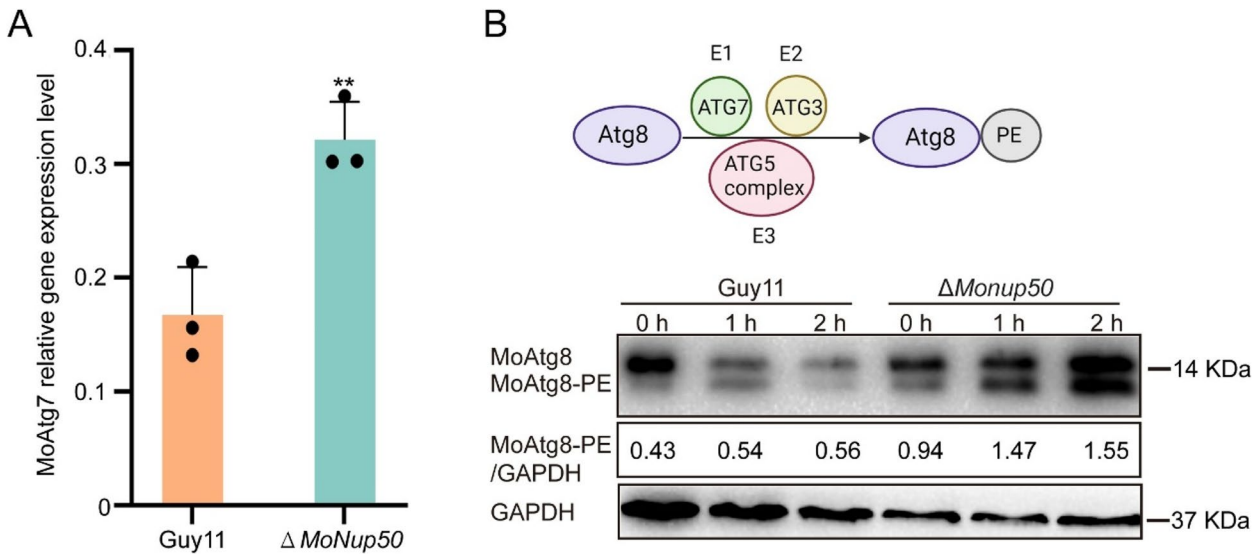

Fig. 11 MoNup50 inhibits the MoAtg8-PE synthesis. **A** Expression level analysis of *MoATG7* by qRT-PCR in the Guy11 and Δ*Monup50*. **B** The MoAtg8/MoAtg8-PE turnover in the Guy11 and Δ*Monup50*

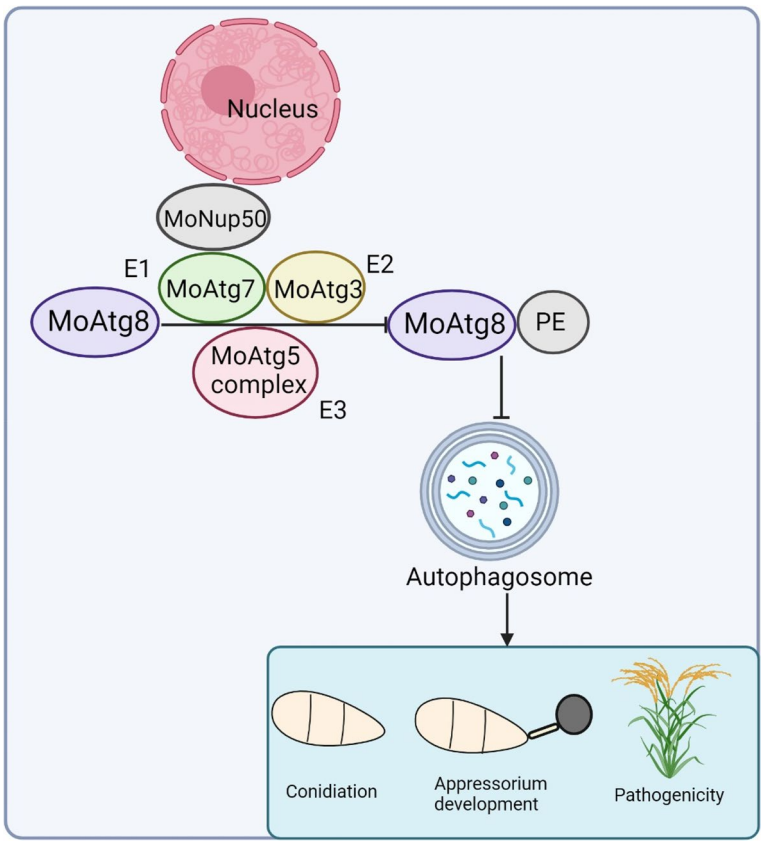

Fig. 12 Model of MoNup50 regulating the synthesis of MoAtg8-PE through its interaction with the key autophagy protein MoAtg7, thereby affecting pathogenicity and autophagy in *M. oryzae*

of *MoNUP50* impaired the transport and degradation of glycogen and lipid droplets, resulting in insufficient turgor pressure in the Δ*Monup50* mutant appressoria. This, in turn, weakened the ability of infectious hyphae to penetrate and expand within the host tissues. In addition to the impact on appressorium function, the integrity of the fungal cell wall is crucial for maintaining turgor pressure in appressorium. The fungal cell wall is a dynamic structure that remodels during fungal development, plant infection, and in response to external stresses [32]. Here, we observed impaired cell wall integrity in the Δ*Monup50* mutant. Growth inhibition assays in the presence of cell wall stressors such as CFW, SDS, and CR showed a significantly higher inhibition rate in the Δ*Monup50* mutant compared to the Guy11 and complemented strains. Furthermore, the Mps1 phosphorylation level was abnormally elevated in the Δ*Monup50* mutant under nutrient-rich and CR-induced cell wall stress conditions. The Mps1 MAPK signaling pathway is known to regulate cell wall integrity, and these results further suggest that MoNup50 is essential for maintaining proper cell wall function. The combined defects in appressorium function and cell wall integrity are likely to contribute to the reduced pathogenicity in the Δ*Monup50* mutant.

Autophagy is a critical process in the fungal pathogenicity. Over the past decade, numerous autophagy-related proteins have been identified in *M. oryzae*, including MoAtg1-MoAtg10, MoAtg12, MoAtg14, MoAtg15, MoAtg16, and MoAtg18. Deletion of any of these key autophagy genes results in the complete loss of pathogenicity [4]. Among these, MoAtg8 serves as a key autophagy marker, with the lipidation of MoAtg8 and the degradation of GFP-MoAtg8 being important indicators of autophagic flux [33]. In our study, we found that the Δ*Monup50* mutant exhibited increased lipidated MoAtg8 accumulation and accelerated GFP-MoAtg8 degradation compared to the Guy11. These results suggest that MoNup50 negatively regulates autophagy in *M. oryzae*, with its deletion resulting in elevated autophagic activity under nutrient-rich and nitrogen-starved conditions. Yeast two-hybrid, GST pull-down, and BiFC assays revealed that MoNup50 interacts with MoAtg7 in vivo and in vitro, suggesting that MoNup50 regulates autophagy by directly affecting the activity of this key autophagy protein.

Atg7 is involved in two ubiquitin-like conjugation pathways, including the conjugation of Atg12-Atg5 and Atg8 to the autophagosome membrane [25, 26]. Atg8, a ubiquitin-like protein, binds to phosphatidylethanolamine (PE) in a process similar to how ubiquitin binds to target proteins [34]. The lipidation of Atg8 to PE requires the E1 activating enzyme Atg7, the E2 conjugating enzyme Atg3, and the E3 complex Atg12-Atg5. In this study, we demonstrated that MoNup50 interacts with MoAtg7 and regulates autophagy through this interaction. The Δ*Monup50* mutant exhibited increased MoAtg8-PE accumulation, further suggesting that MoNup50 modulates autophagy by influencing the lipidation of MoAtg8 [25]. In mammalian cardiomyocytes, the overexpression of *ATG7* induces autophagy [35], while *ATG7* deficiency in mice leads to cellular dysfunction and cell cycle arrest in starved mouse embryonic fibroblasts [36]. In *Nicotiana benthamiana*, overexpression of *ATG7* induces autophagy in plant cells, and Atg7 interacts with several autophagy-related proteins, including Atg3, Atg10, and Atg8 [37]. Interestingly, Atg8 specifically interacts with the C-terminus of Atg7 [38]. In *M. oryzae*, MoAtg7 is critical for pathogenicity, and its deletion results in the complete loss of virulence [39]. These studies highlight the central role of Atg7 in autophagy regulation, particularly in the conjugation of Atg8 to PE, which is essential for autophagosome membrane expansion. Our study further confirms the involvement of MoAtg7 in *M. oryzae* pathogenicity, with MoNup50 influencing its function by regulating the autophagic process through MoAtg7. Recent studies have shown that post-translational modifications of MoAtg7 influence autophagy and pathogenicity in *M. oryzae*. For example, Gcn5, a histone acetyltransferase (HAT) that shuttles between the nucleus and cytoplasm negatively regulates autophagy by acetylating Atg7 [9]. Future studies will explore whether MoNup50 affects the function of MoAtg7 through post-translational modifications, providing deeper insights into the precise mechanisms by which MoNup50 regulates autophagy and pathogenicity.

In conclusion, this study elucidates the critical roles of the nuclear basket nucleoporin MoNup50 in both autophagy regulation and pathogenicity in *M. oryzae*. MoNup50 regulates autophagy homeostasis by interacting with the key autophagy protein MoAtg7, thereby influencing hyphal vegetative growth, sporulation, spore morphology, appressorium formation, appressorium turgor pressure, degradation and transport of appressorium glycogen and lipid droplets, and pathogenicity in *M. oryzae*. Future research will focus on understanding how MoNup50 modulates MoAtg7 function to further refine our understanding of the molecular mechanisms underlying fungal pathogenicity.

Materials and methods

Generation of deletion mutants and complemented strains

Gene knockout was performed using *Agrobacterium tumefaciens*-mediated transformation (*At*MT). The pKO3 A vector was used to construct the knockout vector. The upstream (1.5 kb) and downstream fragments (1.5 kb) of *MoNUP50* were amplified by PCR using specific primers (Table S1). The hygromycin resistance gene fragments (*HPH*) were cloned from pCB1003 using specific primers (Table S1). The upstream fragment, *HPH,* and the downstream fragment were then ligated into the linearized vector pKO3 A (*Hind*III/*Xba*I) using Phanta Max Super-Fidelity DNA Polymerase (Vazyme Biotech co.,ltd). The resulting knockout cassettes were introduced into Guy11 strain by *At*MT. Positive transformants exhibiting *HPH* resistance were selected on media containing hygromycin B (200 μg/mL) and 5-fluoro-2'-deoxyuridine (0.5 μM). Verification of the mutants was conducted using two sets of PCR primers to confirm the deletion of *MoNUP50*.

To generate the gene-complemented strains (Δ*Monup50::MoNUP50*), the *MoNUP50* sequence, along with its native promoter, was fused with the pKD5 vector (*EcoRI* and *SmalI*-linearized) containing the sulfonylurea resistance gene (*SUR*). The gene-complemented plasmids were then introduced into the Δ*Monup50* mutant. Complemented strains (Δ*Monup50::MoNUP50*) were screened using sulfonylurea (100 μg/mL) and confirmed by fluorescence microscopy.

Fungal strains, growth conditions and primers

The *M. oryzae* wild-type strain Guy11 was cultured on complete media (CM) at 25 °C with a 16/8 h light/dark photoperiod. For hyperosmotic stress and cell wall stress experiment, the Guy11, the Δ*Monup50* mutant, and the complemented strains were inoculated onto CM supplemented with 1 M Sorbitol, 0.6 M KCl, 0.6 M NaCl, 50 μg/mL Calcofluor White (CFW), 0.005% SDS and 600 μg/mL Congo Red (CR). All experiments were performed in triplicate. The primers used for PCR amplification in this study are listed in Table S1. Table S2 listing all strains used in this study.

Phenotypic analyses

For growth and conidiation experiments, Guy11, Δ*Monup50* mutant, and complemented strains were inoculated onto quantitative CM medium at 25 °C for 8 days. Colony diameters were measured, and spore production was microscopically quantified. For appressorium-related phenotypic analysis, spores (5×10^4 conidia mL^{-1}) of fungal strains were washed with sterile water, and dropped onto a hydrophobic membrane to induce appressorium formation. Appressorium formation and

collapse were monitored and counted. During appressorium formation, glycogen transport was monitored by staining with KI/I_2 solution, while lipid droplet degradation was observed using BODIPY staining. For pathogenicity experiments, mycelial plugs and spore suspensions (5×10^4 conidia mL^{-1}) of fungal strains were inoculated onto detached barley and rice leaves. Disease progression was observed and photographed 4–5 days post-inoculation. Each experiment was repeated three times.

Yeast two-hybrid assays

To perform yeast two-hybrid assays, the cDNA of *MoNUP50* was cloned into the bait vector pGBKT7. The prey vector was constructed by inserting *MST50* cDNA into pGADT7. The primers used are listed in Table S1. Both vectors were co-transformed into the yeast strain Y2HGold, following the manufacturer's protocol for the Matchmaker Gal4 Two-Hybrid System 3 (Clontech, USA).

In vitro GST pull-down assays

For the in vitro GST pull-down assays, the cDNA of *MoNUP50* was cloned into the SalI/*Hind*III site of pET21a vector to generate the His-MoNup50 plasmid. Similarly, the cDNA of *MoATG7* was inserted into the EcoRI1 site of the pGEX4 T-2 vector (GE Health care Life Science) to generate the GST-MoAtg7 plasmid. Both plasmids were transformed into *Escherichia coli* strain BL21 (DE3) cells. These cells were harvested and resuspended in a lysis buffer containing10 mM Tris–HCl (pH 7.5), 0.5% Triton X-100, 150 mM NaCl and 0.5 mM EDTA. After cell lysis, extracted proteins were analyzed by SDS–PAGE and stained with Coomassie blue. Western blotting was performed to confirm the expression of the target proteins. The GST or GST-MoAtg7 supernatants were incubated with 50 µL glutathione agarose beads (Invitrogen) 4 °C for 2 h. Subsequently, His-MoNup50 bacterial lysate were added and incubated at 4 °C for 1 h. The eluted proteins were then detected by western blotting using anti-GST and anti-His antibodies (Hua An). Table S3 listing all antibodies used in this study.

Bimolecular fluorescence complementation (BiFC) assay

The coding sequences of *MoNUP50* and *MoATG7* were retrieved from the NCBI database, and their coding regions were analyzed using the EnsemblFungi database to determine the positions of their start and stop codons. Amplified *MoNUP50* and *MoATG7* fragments were then cloned into the pKD5 and pKD2 vectors, respectively. The resulting MoNup50-YFPC and YFPN-MoAtg7 constructs were co-transformed into the Guy11 via *At*MT. The positive transformants were selected on plates containing sulfonylurea (100 µg/mL) and hygromycin B (200 µg/mL). YFP signals were detected using a Zeiss LSM880 confocal microscope (Zeiss LSM880).

Phosphorylation analysis

To measure Mps1 phosphorylation levels, total proteins were extracted from Guy11 and Δ*Monup50* mutant using the TCA-acetone method. Protein concentrations were determined using an Enhanced BCA Protein Assay Kit (Beyotime). Phosphorylation of Mps1 was analyzed by western blotting using anti-phospho-p44/42 MAPK antibody and anti-ERK1/2 MAPK antibody (Cell Signaling Technology). Similarly, Osm1 phosphorylation levels were detected using anti-MAPK14 (T180/Y182) antibody and anti-MAPK14 antibody (Cell Signaling Technology).

Autophagy assays

Autophagic activity was assessed using a GFP-MoAtg8 fusion protein with its native promoter, which was transformed into Guy11 and the Δ*Monup50* mutant via *At*MT method. Transformants expressing GFP-MoAtg8 were analyzed by fluorescence microscopy. The degradation of autophagosome was monitored in both mycelia and conidia using fluorescence microscopy. Furthermore, GFP-MoAtg8 degradation was assessed by western blotting, and the levels of MoAtg8-PE in Guy11 and Δ*Monup50* mutants were measured by western blotting after starvation for 0 h, 1 h, and 2 h. Data were analyzed using ImageJ software.

Supplementary Information

The online version contains supplementary material available at https://doi.org/10.1186/s12964-025-02219-7.

Supplementary Material 1.

Supplementary Material 2.

Acknowledgements

We are grateful to all individuals who contributed to this study.

Authors' contributions

Ying-Ying Cai: Investigation, Data curation, Methodology, Writing-original draft. Xue-Ming Zhu, Muhammad Noman, Jing Wang: Investigation, Methodology. Zhong-Na Hao, Yan-Li Wang, Lin Li: Data curation, Methodology. Jian-Ping Lu, Xiao-Hong Liu: Investigation, Writing-review & editing, Methodology. Jiao-Yu Wang, Fu-Cheng Lin: Conceptualization, Writing-review & editing, Funding acquisition, Supervision. All authors reviewed the manuscript.

Funding

This study was supported by the Key Research and Development Project in Zhejiang Province (2023C02018), Natural Science Foundation of Zhejiang province of China (ZCLQN25C0101), National Key Research and Development Program of China (2023YFD1400200), and the National Natural Science Foundation of China (32300169).

Data availability

No datasets were generated or analysed during the current study.

Declarations

Ethics approval and consent to participate
No ethics approval or consent was required since this study did not include patient samples, human subjects, or animal experiments.

Consent for publication
No ethics approval or consent was required since this study did not include patient samples, human subjects, or animal experiments.

Competing interests
The authors declare no competing interests.

Received: 5 December 2024 Accepted: 26 April 2025
Published online: 29 May 2025

References

1. Chen X, Selvaraj P, Lin LL, Fang WQ, Wu CX, Yang P, et al. Rab7/Retromer-based endolysosomal trafficking is essential for proper host invasion in rice blast. New Phytol. 2023;239(4):1384–403.
2. Zhang F, Wang M, Wang GL, Ning YS, Wang RY. Insights into metabolite biosynthesis and regulation in rice immune signaling. Trends Microbiol. 2023;31(3):225–8.
3. Ryder LS, Talbot NJ. Regulation of appressorium development in pathogenic fungi. Curr Opin Plant Biol. 2015;26:8–13.
4. Liu XH, Xu F, Snyder JH, Shi HB, Lu JP, Lin FC. Autophagy in plant pathogenic fungi. Semin Cell Dev Biol. 2016;57:128–37.
5. Eseola AB, Ryder LS, Oses-Ruiz M, Findlay K, Yan X, Cruz-Mireles N, et al. Investigating the cell and developmental biology of plant infection by the rice blast fungus *Magnaporthe oryzae*. Fungal Genet Biol. 2021;154:1–13.
6. Cai YY, Li L, Zhu XM, Lu JP, Liu XH, Lin FC. The crucial role of the regulatory mechanism of the Atg1/ULK1 complex in fungi. Front Microbiol. 2022;13:1–17.
7. Zhu XM, Li L, Wu M, Liang S, Shi HB, Liu XH, et al. Current opinions on autophagy in pathogenicity of fungi. Virulence. 2019;10(1):481–9.
8. He M, Xu Y, Chen J, Luo Y, Lv Y, Su J, et al. MoSnt2-dependent deacetylation of histone H3 mediates MoTor-dependent autophagy and plant infection by the rice blast fungus *Magnaporthe oryzae*. Autophagy. 2018;14(9):1543–61.
9. Zhang SL, Liang ML, Naqvi NI, Lin CX, Qian WQ, Zhang LH, et al. Phototrophy and starvation-based induction of autophagy upon removal of Gcn5-catalyzed acetylation of Atg7 in. Autophagy. 2017;13(8):1318–30.
10. He M, Kershaw MJ, Soanes DM, Xia Y, Talbot NJ. Infection-associated nuclear degeneration in the rice blast fungus *Magnaporthe oryzae* requires non-selective macro-autophagy. PLoS ONE. 2012;7(3):1–17.
11. Mizushima N, Sugita H, Yoshimori T, Ohsumi Y. A new protein conjugation system in human - The counterpart of the yeast Apg12p conjugation system essential for autophagy. J Biol Chem. 1998;273(51):33889–92.
12. Akey CW, Singh D, Ouch C, Echeverria I, Nudelman I, Varberg JM, et al. Comprehensive structure and functional adaptations of the yeast nuclear pore complex. Cell. 2022;185(2):361–78.
13. Zhu XC, Huang GXY, Zeng C, Zhan XC, Liang K, Xu QK, et al. Structure of the cytoplasmic ring of the *Xenopus laevis* nuclear pore complex. Science. 2022;376(6598):1177–88.
14. Lin DH, Hoelz A. The Structure of the Nuclear Pore Complex (An Update). Annu Rev Biochem. 2019;88(88):725–83.
15. Lange A, Fasken MB, Stewart M, Corbett AH. Dissecting the roles of Cse1 and Nup2 in classical NLS-cargo release in vivo. Traffic. 2020;21(10):622–35.
16. Buchwalter AL, Liang Y, Hetzer MW. Nup50 is required for cell differentiation and exhibits transcription-dependent dynamics. Mol Biol Cell. 2014;25(16):2472–84.
17. Suresh S, Markossian S, Osmani AH, Osmani SA. Mitotic nuclear pore complex segregation involves Nup2 in *Aspergillus nidulans*. J Cell Biol. 2017;216(9):2813–26.
18. Wang YX, Zhang CQ, Zhao XZ, Qiu YX, Wang XY, Zhao CZ, et al. The nuclear pore protein Nup2 is essential for growth and development, stress response, pathogenicity and deoxynivalenol biosynthesis in *Fusarium graminearum*. Pest Manage Sci. 2024;81(1):1–11.
19. Tomioka Y, Kotani T, Kirisako H, Oikawa Y, Kimura Y, Hirano H, et al. TORC1 inactivation stimulates autophagy of nucleoporin and nuclear pore complexes. J Cell Biol. 2020;219(7):1–14.
20. Funasaka T, Tsuka E, Wong RW. Regulation of autophagy by nucleoporin Tpr. Sci Rep. 2012;2:1–9.
21. Li GT, Zhou XY, Xu JR. Genetic control of infection-related development in *Magnaporthe oryzae*. Curr Opin Microbiol. 2012;15(6):678–84.
22. de Jong JC, MCCormack BJ, Smirnoff N, Talbot NJ. Glycerol generates turgor in rice blast. Nature. 1997;389(6648):244–5.
23. Nazio F, Cecconi F. Autophagy up and down by outsmarting the incredible ULK. Autophagy. 2017;13(5):967–8.
24. Heitman J, Movva NR, Hall MN. Targets for cell-cycle arrest by the Immunosuppressant Rapamycin in yeast. Science. 1991;253(5022):905–9.
25. Hanada T, Noda NN, Satomi Y, Ichimura Y, Fujioka Y, Takao T, et al. The Atg12-Atg5 conjugate has a novel E3-like activity for protein lipidation in autophagy. J Biol Chem. 2007;282(52):37298–302.
26. Mizushima N, Noda T, Yoshimori T, Tanaka Y, Ishii T, George MD, et al. A protein conjugation system essential for autophagy. Nature. 1998;395(6700):395–8.
27. Nair U, Yen WL, Mari M, Cao Y, Xie Z, Baba M, et al. A role for Atg8-PE deconjugation in autophagosome biogenesis. Autophagy. 2012;8(5):780–93.
28. Floch AG, Palancade B, Doye V. Fifty years of nuclear pores and nucleocytoplasmic transport studies: multiple tools revealing complex rules. Nuclear Pore Complexes Nucleocytoplasmic Transport - Methods. 2014;122:1–40.
29. Park SJ, Son SM, Barbosa AD, Wrobel L, Stamatakou E, Squitieri F, et al. Nuclear proteasomes buffer cytoplasmic proteins during autophagy compromise. Nat Cell Biol. 2024;26(10):1691–9.
30. Zhu XM, Li L, Bao JD, Wang JY, Liang S, Zhao LL, et al. MoVast2 combined with MoVast1 regulates lipid homeostasis and autophagy in. Autophagy. 2023;19(8):2353–71.
31. Howard RJ, Valent B. Breaking and entering: Host penetration by the fungal rice blast pathogen *Magnaporthe grisea*. Annu Rev Microbiol. 1996;50:491–512.
32. Yin ZY, Feng WZ, Chen C, Xu JY, Li Y, Yang LN, et al. Shedding light on autophagy coordinating with cell wall integrity signaling to govern pathogenicity of *Magnaporthe oryzae*. Autophagy. 2020;16(5):900–16.
33. Klionsky DJ, Abdel-Aziz AK, Abdelfatah S, Abdellatif M, Abdoli A, Abel S, et al. Guidelines for the use and interpretation of assays for monitoring autophagy (4th edition)(1). Autophagy. 2021;17(1):1–382.
34. Ichimura Y, Kirisako T, Takao T, Satomi Y, Shimonishi Y, Ishihara N, et al. A ubiquitin-like system mediates protein lipidation. Nature. 2000;408(6811):488–92.
35. Pattison JS, Osinska H, Robbins J. Atg7 induces basal autophagy and rescues autophagic deficiency in CryABR120G cardiomyocytes. Circ Res. 2011;109(2):151–60.
36. Lee IH, Kawai Y, Fergusson MM, Rovira II, Bishop AJ, Motoyama N, et al. Atg7 modulates p53 activity to regulate cell cycle and survival during metabolic stress. Science. 2012;336(6078):225–8.
37. Yang M, Zhang Y, Xie X, Yue N, Li J, Wang XB, et al. Barley stripe mosaic virus γb Protein Subverts Autophagy to Promote Viral Infection by Disrupting the ATG7-ATG8 Interaction. Plant Cell. 2018;30(7):1582–95.
38. Hong SB, Kim BW, Lee KE, Kim SW, Jeon H, Kim J, et al. Insights into noncanonical E1 enzyme activation from the structure of autophagic E1 Atg7 with Atg8. Nat Struct Mol Biol. 2011;18(12):1323–30.
39. Kershaw MJ, Talbot NJ. Genome-wide functional analysis reveals that infection-associated fungal autophagy is necessary for rice blast disease. Proc Natl Acad Sci USA. 2009;106(37):15967–72.

Publisher's Note